ARTICLE   OPEN

Check for updates

Chest-scale self-compensated epidermal electronics for standard 6-precordial-lead ECG

Lang Yin [1,2,3], Youhua Wang [1,2,3], Jian Zhan [1,2], Yunzhao Bai [1,2], Chao Hou [1,2], Junfeng Wu [1,2], Rong Huang [1,2], Yuzhou Wang [1,2] and YongAn Huang [1,2 ✉]

Six chest leads are the standardized clinical devices of diagnosing cardiac diseases. Emerging epidermal electronics technology shift the dangling wires and bulky devices to imperceptible wearing, achieving both comfortable experience and high-fidelity measuring. Extending small areas of current epidermal electronics to the chest scale requires eliminating interference from long epidermal interconnects and rendering the data acquisition (DAQ) portable. Herein, we developed a chest-scale epidermal electronic system (EES) for standard precordial-lead ECG and hydration monitoring, including the only μm-thick substrate-free epidermal sensing module and the soft wireless DAQ module. An electrical compensation strategy using double channels within the DAQ module and epidermal compensated branches (ECB) is proposed to eliminate unwanted signals from the long epidermal interconnects and to achieve the desired ECG. In this way, the EES works stably and precisely under different levels of exercise. Patients with sinus arrhythmias have been tested, demonstrating the prospect of EES in cardiac diseases.

INTRODUCTION

Clinically standardized chest leads extensively distribute from right chest to under the left armpit (Supplementary Fig. 1), observing the electrical activities within the heart from multi-views, being an essential way for screening and diagnosing cardiac diseases[1,2]. How to obtain comprehensive electrocardiogram (ECG) using portable devices has been an increasing concern for investigation. However, the stiff data acquisition (DAQ) module and electrodes as well as long tangling wires of commercial portable devices, including 12-lead ECG monitors[3], Holter monitors[4], are unfriendly to users' experience.

With the progression of flexible materials[5–7] and mechanical designs[8–10], the wireless integrated epidermal electronic system (EES)[11–15] has attracted more and more researchers' interest. The flexible electrodes can be transferred[16,17] or directly sintered[18,19] onto the time-dynamic and curvilinear skin, facilitating the acquisition of high-fidelity biosignals. They have been popularly used in the fields of human-computer interaction[20–23], medical health[24–27], and bioengineering[28–31]. Applying EES to wearable precordial-leads ECG monitoring needs to scale up the size from centimeters to decimeters, so that the ECG of 6 chest leads can be acquired simultaneously. At present, some state-of-the-art studies[32–34] that are applicable for multi-lead ECG acquisition primarily focus on the preparation of large-area flexible electrodes. However, simply expanding the size of EES cannot accurately obtain the 6-chest-lead ECG. This is attributed to the increasingly long exposed epidermal interconnects (EEIs) that accompany the increased size of the EES. The EEIs can capture unwanted non-negligible biopotentials, which cannot be directly eliminated by data processing in software of back-end. The potential of EEIs are mixed with the target signal of ECG electrodes, resulting in that the ECG is record by the whole wire-like electrodes rather than the target electrodes in the standard leads position. Present solution to this problem can be broadly classified in two categories:

(1) Insulate the EEIs form skin using dielectric encapsulation layer[12,32,33,35,36]. However, this method only ensures physical insulation, while the electrical insulation effect largely depends on the thickness of the dielectric layer. If a thin dielectric layer is used, a capacitive will be formed between the electrode and the skin, which means the biopotential of EEIs can still be acquired[37]. On the contrary, if a thick dielectric layer is used, the stiffness of the epidermal electrodes will increase dramatically, and thus cannot make conformal contact with the skin texture (the critical thickness is about 25 μm)[38]. In short, this strategy is contradictory in terms of device flexibility and insulation effect.

(2) Electrically compensate the EEIs. We have previously proposed a fully electrical compensation method[39] (here we name front-end compensation) which has been demonstrated to be effective in eliminating the potential of EEIs. This method completely relies on the structural design of the front end (epidermal sensing module), which introduces the design of extra epidermal compensation electrodes (ECEs). However, the ECEs need to be connected in series with EEIs and be in a stable biopotential. The stringent requirement is difficult to meet in practice and is not conducive to the integration of EES. This inspired us to investigate a different compensation method suitable for system-level integration.

To solve the problems above and achieve accurate wearable monitoring of 6-precordial-lead ECG, this paper introduced the large-area (248 mm × 112 mm) and sweat/heat-permeable EES, integrating the epidermal sensing module and the soft wireless DAQ module. Six filamentary epidermal electrodes of the epidermal sensing module are attached on the locations of standard precordial leads, and connected to the soft DAQ module by the long EEI. The interference signals from the EEI are removed

[1]State Key Laboratory of Digital Manufacturing Equipment and Technology, Huazhong University of Science and Technology, Wuhan 430074, China. [2]Flexible Electronics Research Center, Huazhong University of Science and Technology, Wuhan 430074, China. [3]These authors contributed equally: Lang Yin, Youhua Wang.
✉email: yahuang@hust.edu.cn

npj

elegantly by a compensation strategy, i.e., co-front-back compensation, which uses a combination of double channels within the DAQ module and epidermal compensation branches (ECBs). The compensation strategy shows higher compensation accuracy and easier integration with the wireless module than the previous front-end compensation strategy. This EES has exhibited significant advantages in perspiration, heat dissipation, and signal accuracy. The applications were successfully verified in scenarios such as human movement, heat and cold stimulation, and disease screening, aiming to provide a comprehensive wearable cardiac health management strategy.

RESULTS

Design of the EES

Figure 1a depicts the EES with self-compensation part that is integrated on human body. First, the cardiomyocyte depolarization followed by repolarization during each cardiac cycle renders a potential difference between the inside and outside of the cell membrane. The processes occur sequentially from the endocardium to the epicardium, composing the ECG on human skin. The time-dynamic ECG is recorded from the position of 6 precordial leads (V1–V6) by the EES designed according to the subject's somatotype (including an epidermal sensing module and a soft DAQ module, shown in Supplementary Fig. 2). The epidermal sensing module of the EES consists of two parts (Supplementary Fig. 3): the ECG part that contains the epidermal working electrodes (EWEs) with EEIs and ECBs for the 6 precordial leads; and the hydration part that contains the reference (REF) electrode, ground (GND) electrode, and epidermal hydration sensor. The location of GND/REF electrodes is designed close to the abdomen, where the heart is far away and few muscles are involved within the scope of chest-scale integration, and thus can be approximately considered to have a relatively stable potential. The wireless DAQ module is broken down into the data acquisition part and WiFi transmission part, which are connected by pins. Usually, the potential introduced by the inevitable EEIs may cause the actual ECG to deviate from those of the ideal precordial leads. To solve this problem, a co-front-back compensation strategy is proposed. The front end (the epidermal sensing module) designs ECBs in parallel with EEIs. The back end (the soft DAQ module (Fig. 1b) and the user interface) acquires the signals from front-end epidermal sensing modules by double channels and linear superposition them. Through the co-compensation of front end and back end, the interference signals from the EEIs can be completely eliminated: the ECG after co-front-back compensation is basically the signal from the EWEs, which is the same as the ideal ECG. In this way, the 6-precordial-leads ECG and hydration monitoring can be performed on portable devices such as laptops and cell phones.

The workflow of the EES is illustrated in Fig. 1c. The workflow is divided into two blocks according to the type of sensors: one is the ECG function block, which contains two parts of signals: the 6-channel differential signal between the EWEs/EEIs and the reference electrode (i.e., EWE/EEI-REF); and another is the 6-channel differential signal between the EWEs/EEIs and the ECB (i.e., EWE/EEI-ECB). Both parts of signals are amplified, filtered, and analog-to-digital converted in the same way and wirelessly sent to the host computer via WiFi for 12 channels of ECG in total. Those two parts of signals are linearly combined by compensation algorithms. The baseline wandering, high-frequency noise, and a power noise of 50 Hz are eliminated via a high-pass filter with the cutoff of 0.05 Hz, low-pass filter with the cutoff of 200 Hz, and a notch filter of 50 Hz, respectively. The filtered data are smoothing via a moving average of 0.01 s. In this way, the information such as heart rate and heart disease can be extracted through the

standard ECG[2]. The second block is the hydration function block, from which the signals are measured by a dedicated impedance-measurement chip and sent to the host computer for processing together with the ECG. The final user interface (Supplementary Fig. 4) includes a real-time display of the final results of both 6-leads ECG, heart rate, and hydration index.

Figure 1d shows the ultra-thin epidermal sensors with their thickness being 1.6 μm (including 150-nm-thick Au, 10-nm-thick Cr, and 1.5-μm-thick polyethylene terephthalate (PET)) laminated on human skin. The flexibility of epidermal sensors can sustain the different skin deformation (e.g., compression, stretching, and shearing) and chest movement (e.g., chest enlargement and retraction) (Supplementary Fig. 5), even to be wrapped around a hair strand with its surface fully conforming to the hair (Fig. 1e). Nevertheless, we adopted a more compact design for the wireless DAQ module based on the commercial flexible printed circuit board (FPCB). This is due to the fact that current flexible circuit manufacturing methods (e.g., serpentine interconnects, elastomer packages, etc.) limit the level of integration and functional complexity that can be achieved[40]. The full flexibilization would considerably increase the area of the wireless DAQ module for the 12-channel voltage and 1-channel impedance-measurement requirements in this paper (Supplementary Fig. 6). Therefore, more consideration needs to be given to the relatively rigid DAQ module in terms of placement and connection to the epidermal sensing module. Based on the chest strain map[41], we designed the DAQ module below the pectoral muscle, where the strain is relatively low compared to other regions and convenient to integrate with the epidermal electrodes at V1–V6. To further enhance the stability of the connection between the soft DAQ module and the epidermal sensing module, we propose a transition connection based on a suspended liquid metal (Fig. 1f). The structure takes advantage of the high surface tension of liquid metal to form a suspended liquid metal droplet (Supplementary Fig. 7a) for the cushion between the DAQ module and the epidermal sensing module. This liquid metal transition connection is more stable compared to the welding method (Supplementary Fig. 7b). We simulated the normal and tangential motions applied to the connection by vertical and horizontal vibrations of the electromagnetic vibration test stand (YDC-0500, Yibofan, China). As shown in Supplementary Fig. 7c, d, the connection by direct welding has a higher probability of disconnection when subjected to low-frequency vibration and is negatively correlated with the vibration frequency, while the vibration intensity has little effect on it (the lowest vibration intensity of the test stand is sufficient for its disconnection). In contrast, the liquid metal transition connection showed stable conductivity under various of vibration conditions (Supplementary Fig. 7e, f), demonstrating the possibilities in mobile wearable ECG monitoring. Even though the liquid metal is corrosive against metals[42,43], the presence of the generated alloy maintains a decent electrical conductivity after 12 h of corrosion (Supplementary Fig. 8), which is acceptable for disposable epidermal electrodes.

Theoretical modeling and validation of signal compensation

Precordial leads composed of 6 leads are positioned over a wide span of dozens of centimeters, from the right chest to below the center point of the axilla, hence the EEI directly attached on the skin are much longer than the EWE. Correspondingly, it cannot ignore that the targeted ECG signals collected by EWEs are overwhelmed by those from EEIs. It is worth noting that the signal acquired on the EEI is generally similar to the target signal and thus has a resemblance of the response in the spectrum (Supplementary Fig. 9), which means that it cannot be removed simply by signal conditioning such as filtering.
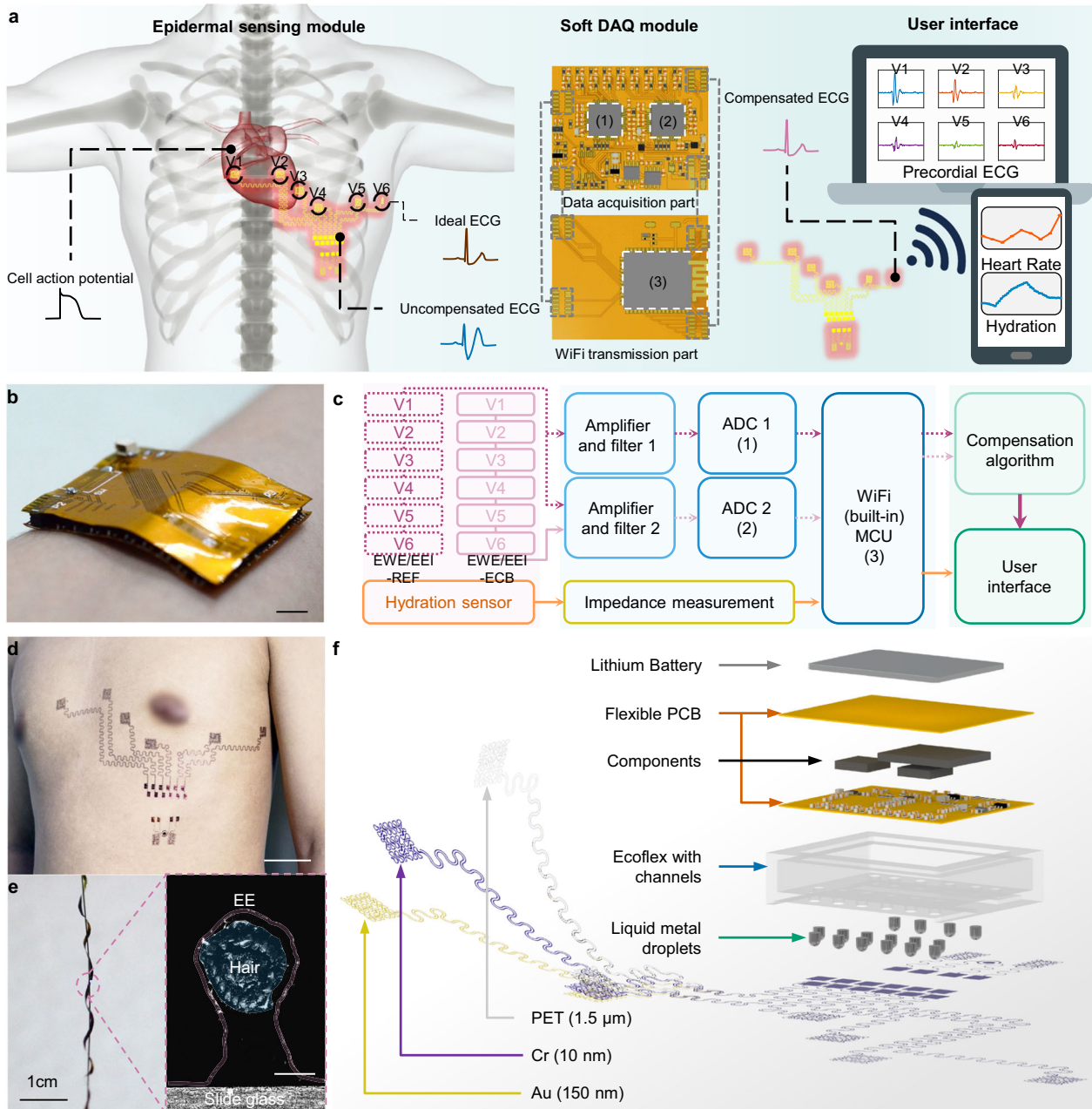
Fig. 1 The architecture of the EES. a Schematic illustration of the EES, including the epidermal sensing module, the soft DAQ module, and the user interface. **b** Wireless DAQ module laminated on the arm. Scale bar, 10 mm. **c** System-level workflow diagram of the EES, showing analog signal acquisition, procession, wireless transmission, compensation algorithm paths from sensor array to the customized user interface (numbers in parentheses indicate the corresponding labeled components in (**a**). **d** The photograph of a participant wearing the epidermal sensors. Scale bar, 50 mm. **e** Optical and microscopic images of filamentary epidermal sensors wrapped around a hair strand. The scale bars on the left and right panel are 1 cm and 30 μm, respectively. **f** Components and interconnections of the EES.

To satisfy the integration design, we propose a kind of co-front-back compensation theory (Fig. 2a) to eliminate the interference of EEIs. Here, one chest lead consists of an EWE, an EEI and an ECB. The commonly used lumped-parameter equivalent circuits of the skin-electrode interface[44,45] overlook the dimension effect and therefore we developed the distributed-parameter equivalent circuit in our previous work[39], which carefully considers the size of electrodes. According to the distributed-parameter model, one differential channel connecting to the EEI and ground collects the total ECG of the EEI and the EWE, or the so-called uncompensated ECG, as we discussed in the previous work[39]:

$$V_{\text{uncompensated}} = V_{EWE} \frac{\int_{L_1}^{L_1+L_2} \frac{1}{z} dl}{\int_0^{L_1+L_2} \frac{1}{z} dl} + V_{EEI} \frac{\int_0^{L_1} \frac{1}{z} dl}{\int_0^{L_1+L_2} \frac{1}{z} dl} \quad (1)$$

$$V_{EWE} = \frac{\int_{L_1}^{L_1+L_2} \frac{E}{z} dl}{\int_{L_1}^{L_1+L_2} \frac{1}{z} dl} \quad (2)$$

$$V_{EEI} = \frac{\int_0^{L_1} \frac{E}{z} dl}{\int_0^{L_1} \frac{1}{z} dl} \quad (3)$$

where L_1 and L_2 are the length of EEI and the EWE, respectively. z is the unit cross-sectional area impedance. V_{EWE} and V_{EEI} are the
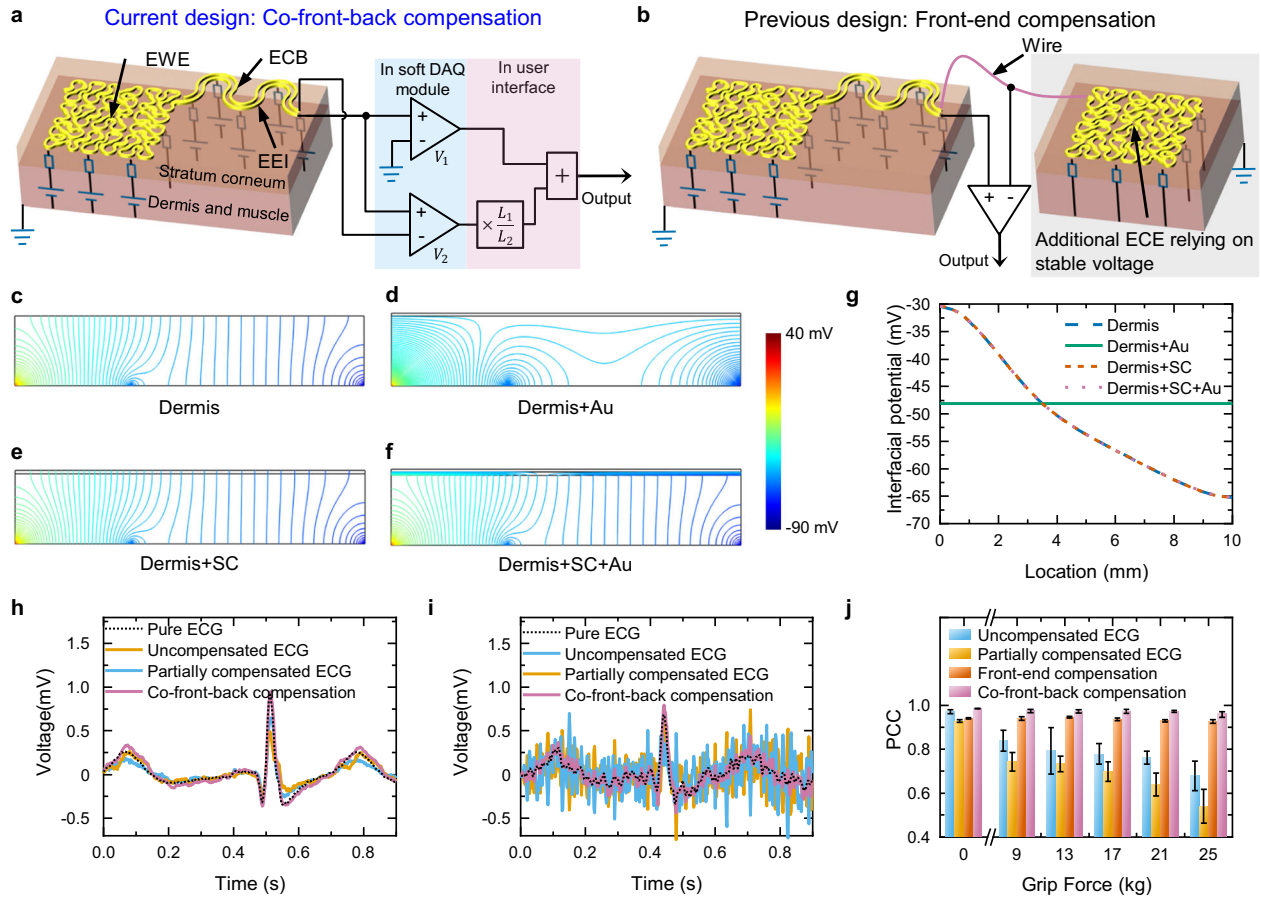
Fig. 2 Signal compensation model and experimental validation. a Schematic of co-front-back compensation. **b** Schematic of front-end compensation proposed in the previous work. **c** The potential distribution in dermis without stratum corneum. **d** The potential distribution in dermis covered with a layer of gold (Au). **e** The potential distribution in dermis covered with stratum corneum. **f** The potential distribution in dermis covered with two layers of SC and Au. **g** Interfacial potential of dermis extracted from **c–f**. **h** ECG measured with forearm relaxed. **i** ECG measured with forearm gripping. **j** Pearson correlation coefficient (PCC) with respect to grip force. Error bars represent the standard deviation of 3 measurements.

voltages acquired by the EWE and EEI, respectively. V_{EWE} is the desired signal from the EWE. Another differential channel connecting to the EEI and the parallel ECB are used to get the partially compensated signals[39]:

$$V_{\text{partially compensated}} = V_{EWE} \frac{\int_{L_1}^{L_1+L_2} \frac{1}{z} dl}{\int_0^{L_1+L_2} \frac{1}{z} dl} - V_{EEI} \frac{\int_{L_1}^{L_1+L_2} \frac{1}{z} dl}{\int_0^{L_1+L_2} \frac{1}{z} dl} \qquad (4)$$

the compensated signals result from the linear combination of both channels as:

$$V_{EWE} = V_{\text{uncompensated}} + \delta V_{\text{partially compensated}} \left(\delta = \frac{L_1}{L_2}\right) \qquad (5)$$

where δ is a dimensionless parameter up to the length ratio of the EEI and the EWE. The linear combination can be automatically calculated in software, such as Labview or Matlab. In conclusion, by close collaboration with the ECB parallel with EEI in the sensing module, the double channels in the DAQ module and linear combination in the software, the interfere of EEI can be theoretically removed.

Our previous front-end compensation strategy (Fig. 2b) requires an extra ECE for each lead. The electrical potential beneath ECEs has to be stable. The locations with stable electrical potentials are generally far from heart, unsuitable for integration with the wireless DAQ module. In contrast, the current co-front-back compensation strategy enhances in integration by replacing ECEs with double channels.

The distributed-parameter equivalent circuit is the fundament of the compensation strategy and the core assumption considers the conductivity of stratum corneum is so weak that the interfacial potentials between dermis and stratum corneum are regarded as voltage sources. Figures 2c to 2f simulate the potential distributions in dermis under various conditions. Comparing Fig. 2c, the lamination of Au electrodes on dermis evidently changes the potential distribution due to its high conductivity, as shown in Fig. 2d, while the existence of the thin stratum corneum maintains the original distribution even a layer of Au laminates on stratum corneum (Fig. 2e, f). Figure 2e exactly plots the interfacial potentials extracted from the top of dermis. It is clear that the stratum corneum with ultralow conductivity does not affect the interfacial potentials of dermis, thus the interfacial potentials can reasonably be seen as voltage sources once the gold electrodes are laminated on the skin. More details of the simulations can be found in the section Methods.

To validate the co-front-back compensation strategy and compare the performance of co-front-back compensation and front-end compensation, a carefully designed experiment was carried out to collect the pure ECG as the standard, the uncompensated ECG polluted by EMG, the partially compensated ECG and the ECG compensated by co-front-back compensation and front-end compensation, respectively. The details are seen in the section Materials and Methods. The primary idea is that the ECG signals as the targeted signals are collected by EWEs and the surface electromyogram (EMG) signals as the interferential signals
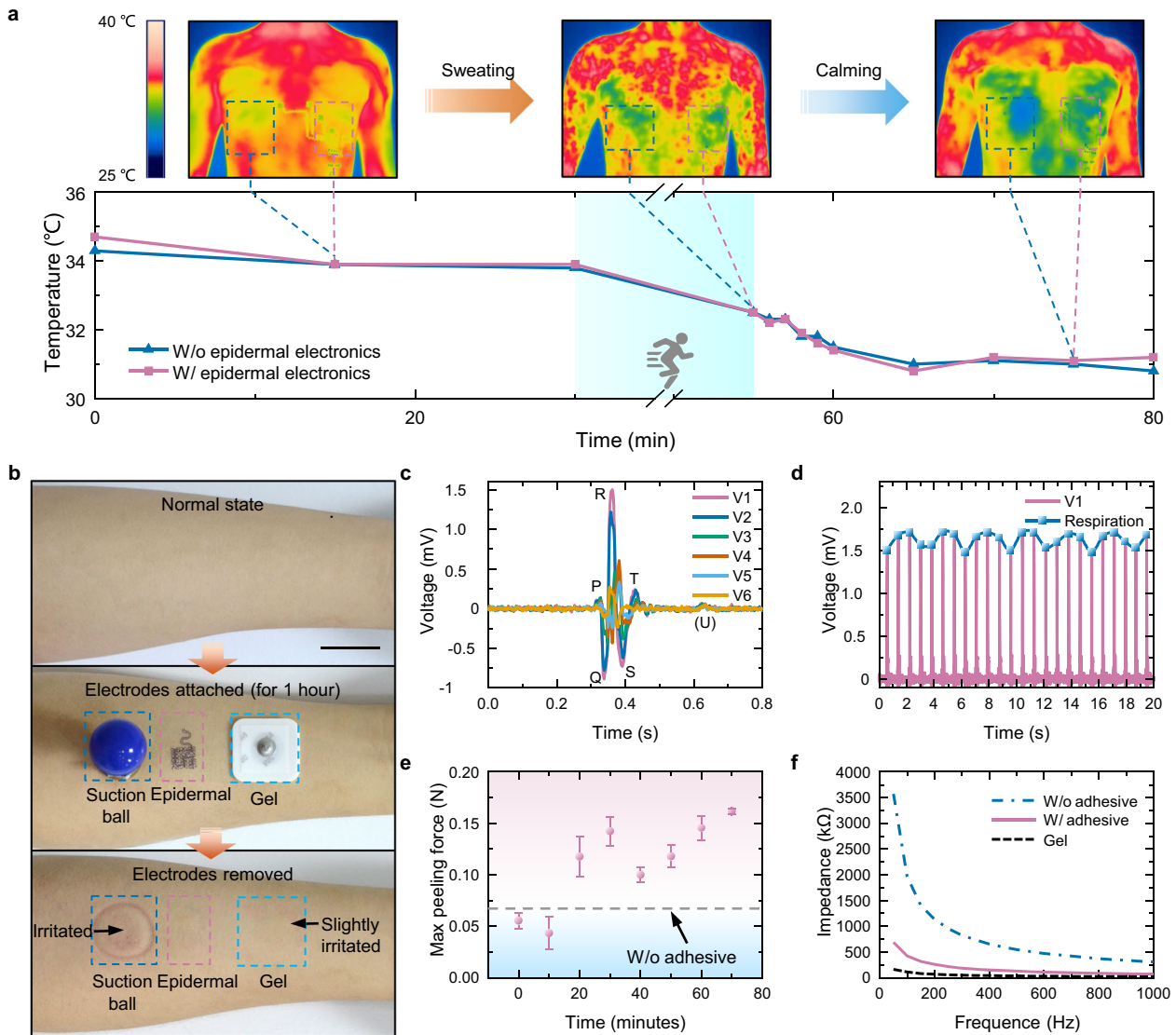
Fig. 3 The result of characterization of epidermal sensors. a Comparison of the skin temperature during running with and without epidermal sensors attached. **b** Comparison of skin irritation by different electrodes: suction ball electrode, epidermal electrode, and gel electrode. Scale bar, 3 cm. **c** V1–V6 ECG acquired by EES. **d** Continuous ECG and respiratory wave. **e** Changes in the maximum adhesion force of skin-epidermal sensors over time after application of mask essence water as a bonding agent. Error bars represent the standard deviation of 3 measurements. **f** Comparison of skin impedance of epidermal electrodes with and without adhesive as well as gel electrodes.

are collected by EEIs and eliminated co-front-back compensation and front-end compensation. The measured ECG are plotted in Fig. 2h, i. The black, orange, blue, and violet curves represent pure, uncompensated, partially compensated, and compensated ECG, respectively. There is no any EMG in each curve when the forearm relaxed (Fig. 2h). Once the muscles are contracted by hand griping, EMG appears in the uncompensated and partially compensated ECG. On the contrary, with the co-front-back compensation strategy, the EMG is cleaned out in the compensated ECG (Fig. 2i and Supplementary Video 1), which successfully validates the co-front-back compensation strategy. To furthermore quantificationally characterize the effectiveness of the compensation strategies, the Pearson correlation coefficient (PCC) is used to compare the similarity between the pure ECG and the collected ECG. The results in Fig. 2j show that with the grip force increasing from 0 to 25 kg, the PCC of uncompensated and partially compensated ECG decreases from larger than 0.9 to 0.54 and 0.67, respectively, indicating the EEI collects more EMG. In contrast, no matter how the grip force is, both compensation

strategies keep larger than 0.9 and the co-front-back compensation strategy is slightly higher than the front-end compensation strategy. The PCC values of the front-end compensation strategy are lower because the potentials beneath ECEs are hard to keep stable. Interestingly, the PCC of both uncompensated and partially compensated ECG are remarkably affected by the fluctuation of EMG (the standard errors are up to 0.11 and 0.08, respectively) while both compensation strategies greatly suppress the fluctuation (the standard errors are about 0.01). As for variable movement introducing forearm deformation, the compensation theory is also valid (Supplementary Fig. 10). The stronger the sEMG of these movements (e.g., twisting), the more pronounced the improvement of PCC by compensation.

Characterization of epidermal sensors

In the long-term wearing of large-area sensors, breathability directly affects the experience of the subjects. Therefore, large-area of the continuous lamellar substrate of the epidermal sensors is removed via slight modified cut and paste process[39]. As a result,
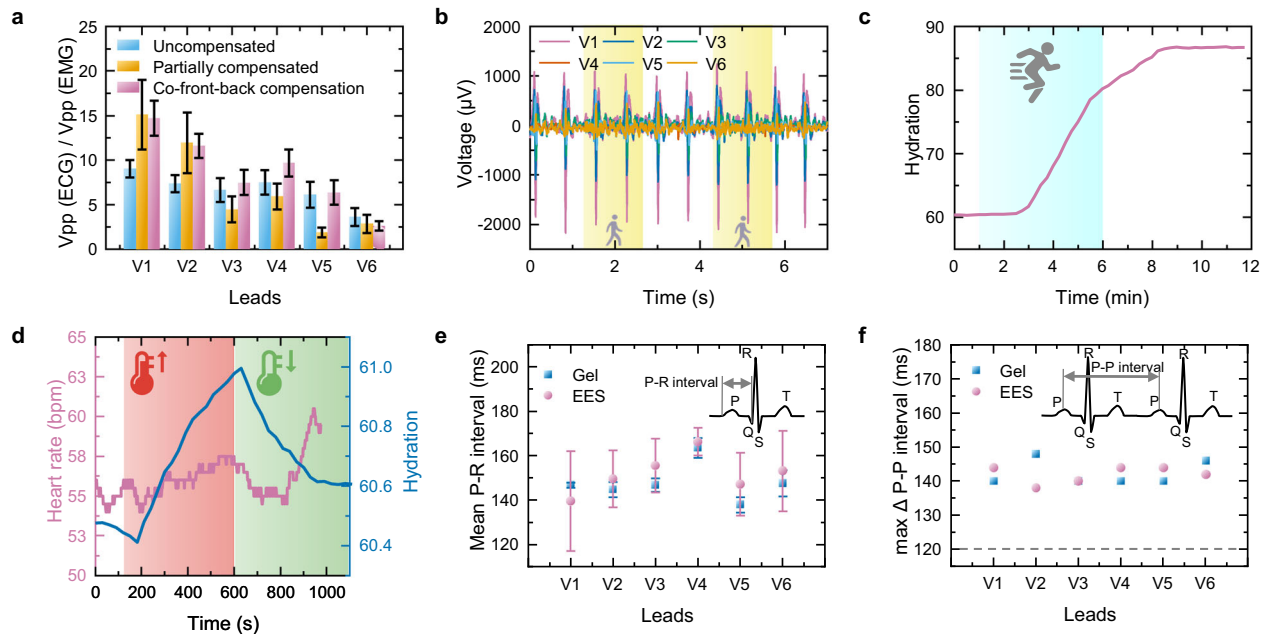
Fig. 4 EES in motion, temperature change, and disease screening. a Comparison of ECG and EMG intensity from V1 to V6 during chest exertion. Error bars represent the standard deviation of 3 measurements. **b** ECG during slow walking. **c** Hydration during running. **d** Heart rate and hydration index during environment temperature change. **e** Mean P-R interval over 5 cardiac cycles extracted by V1–V6 ECGs of the subject with sinus arrhythmia, measured by EES and gel electrodes respectively. Error bars represent the standard deviation of the results from 5 different cardiac cycles. **f** The difference between the maximum and minimum P-P interval extracted from the same ECGs as (**e**).

the filamentary epidermal electronics have significantly more advantages in skin perspiration and heat dissipation than the epidermal electronics with substrate[15,46,47], which have been demonstrated in our previous work[39]. Furthermore, the breathability of this filamentary epidermal electronics in practical usage was investigated (Fig. 3a). Under the following two premises: first, the epidermal electronics are mainly distributed in the left chest; second, the skin temperature is generally symmetric about the central axis of the body under normal conditions. It is reasonable to consider that the average temperature at the right chest (blue dashed box) could represent the skin temperature without epidermal electronics, while the average temperature at the left chest (red dashed box) could represent the skin temperature with epidermal electronics. In the experiment, the epidermal electronics were customized and attached to the subject according to somatotype of users. Then the subject was asked to rest shirtless for 30 min, followed by jogging for 25 min, and finally stopped running and rested for 25 min to calm down. During the whole process, the overall temperature decreased significantly after jogging and eventually stabilized. It can be clearly observed that the average skin temperature of the chest with epidermal electronics attached was almost the same as the temperature of the part without epidermal electronics attached. This is because sweating is the primary heat dissipation way during exercise, thus demonstrating that the epidermal electronics will not hinder skin perspiration. In addition to breathability, another advantage of the substrate-free epidermal electronics is minor skin irritation. Figure 3b compares the skin irritation with two other commercial electrodes (suction bulb electrode (15572, Redy-Med) and gel electrode (2228, 3M, Germany)) after different electrodes being applied for 1 h. The suction bulb electrode caused the most severe irritation to the skin because of a sustained local vacuum on the skin. Similarly, the gel electrode also caused some slight irritation because of prolonged adhesion, while the epidermal electrode caused little. In conclusion, the breathable, non-intrusive nature of the epidermal sensors provides the user with an imperceptible wearing experience.

The ECG acquired by the EES is essentially the same as that acquired by the 'gold standard' gel electrode (Supplementary Fig. 11a). By comparing the effective voltage of the ECG action time to that of the interval, the signal-to-noise ratio can be quantitatively evaluated (Supplementary Fig. 11b). Both signal-to-noise ratios were greater than 25 dB, allowing the acquisition of high-fidelity ECG. Figure 3c shows the compensated ECG of V1–V6 acquired by EES, and the standard ECG features could be observed, including P wave, QRS complex, and T wave, corresponding to atrial depolarization, ventricular depolarization, and ventricular repolarization, respectively. For example, the amplitude of S waves became weaker from V1 to V6, which demonstrates the accuracy of 6-precordial-lead ECG measured by epidermal electronics. In addition, The ECG for a period of time was recorded (Fig. 3d). The amplitude of the R wave fluctuated periodically, coinciding with respiration. This is due to the periodic movement of the chest surface closer to and away from the heart with the contraction and expansion of the chest cavity, resulting in a change in the impedance between the heart and the epidermal electrodes[48]. Therefore, the respiratory wave could be extracted from the ECG, which is also expected to be helpful in respiratory-related diseases (e.g., respiratory arrest).

Stable signals would not be achieved without a reliable electrode-skin contact interface. So an adhesive material was introduced to enhance the adhesion between the epidermal electrodes and the skin without diminishing biocompatibility. We got inspired by a commonly used hydrating mask (Pechoin, China): the mask is usually slippery when first applied, but after skin absorbing for some time, it becomes sticky instead because of the evaporation of moisture in the mask essence. This change was quantified by the test of maximum adhesion force between the skin and epidermal sensors (Fig. 3e). It can be seen that the adhesion force decreased when the mask essence was first applied, at this time, the mask essence played a role in lubrication. 20 min later, the adhesion force rose significantly from 0.05 N to 0.15 N, becoming much larger than that without the mask essence, indicating that the mask essence mainly plays a bonding

role at this time. The change of adhesion force also provided a suitable process window for transferring to skin: apply the mask essence to the chest for more than 20 min before transferring the epidermal electronics to the skin. Nevertheless, in low humidity environments (air conditioning dehumidification mode), the suitable time window will appear in advance to ~10 min (Supplementary Fig. 12). On the one hand, the main component of the mask essence is protein, which has natural biocompatibility. On the other hand, the biocompatible bonding agent can also reduce the skin impedance due to the hydrating effect on the skin. Figure 3f compares the effect of the mask as a bonding agent on the contact impedance. The use of mask essence as an adhesion agent can greatly reduce the contact impedance between the epidermal electrode and the skin, bringing it closer to the level of commercial wet electrodes (gel electrodes). The impedance reduction effect of mask essence can remain relatively stable in the long-term test of 6 h in both normal and dry environment (Supplementary Fig. 13). The quality of the ECG was demonstrated to be related to the electrode-skin interface impedance, which means that this is also beneficial for high-fidelity ECG acquisition.

Application of EES

During human movement, ECG are mixed with the EMG from the pectoral muscle. The relative ratio of EMG to ECG on long EEIs tends to be larger than that of EWEs (EEIs are usually more distant from the heart), which means that eliminating the signal on EEIs by our co-front-back compensation is beneficial for ECG acquisition during pectoral muscle exertion, and we verified this idea experimentally. Figure 4a shows the comparison of ECG and EMG intensities during pectoral muscle exertion. It is noteworthy that an increase in the ECG to EMG ratio occurred in most leads after co-front-back compensation compared to the uncompensated signal (except for V6, which is on the side of the body with little EMG of chest muscle collected). The reason for this phenomenon may be due to the different strengths of the ECG and EMG on EWEs and EEIs: the ECG is stronger the closer to the heart, and the EMG is strong upon the pectoralis major muscle. Based on these properties, we summarized the strength of the potential composition at different sites, as shown in Supplementary Table 2. The co-front-back compensation can eliminate the signal on the EEI, thus improving the ECG/EMG to some extent. The effect of this strategy is particularly prominent in positions with strong EMG such as V1 and V2. However, as shown in Eq. (4), the partially compensated ECG is the difference between EWE and EEI, i.e., the similar potential components of EWE and EEI will be suppressed while the dissimilar parts will be retained. Therefore, ECG/EMG saw a significant decrease where there is a large difference in EMG of EWEs and EEIs (e.g., V3–V6). This result further validates the compensation theory and also illustrates that, since EWEs are typically closer to the heart, the co-front-back compensation is mostly beneficial for ECG acquisition.

One of the advantages of EES is the ability of mobile healthcare. Since the epidermal sensing module and the soft wireless DAQ module are integrated wirelessly, it is possible to record the ECG and hydration simultaneously while moving. Supplementary Video 2 is the actual ECG of lead V1 while strolling, which was stable in the whole movement. Figure 4b shows a segment of the walking ECG. The ECG remained basically stable throughout the time, and the slight EMG were captured when the arm was swinging while walking. In addition to ECG, hydration index can also be monitored simultaneously during running (Fig. 4c). The hydration index saw a rapid increase during running which was attributed to the lowering skin impedance due to sweating. Finally, the hydration index stabilized at a higher level as sweat further saturated. These experiments demonstrate that the EES works properly even when the users are in motion.

Figure 4d shows the changes in heart rate as well as hydration index measured by EES during the dramatic increase and decrease in room temperature. During the 100–600 s, when the temperature rose rapidly, the subject's heart rate began to increase slowly (from 54 to 58 bpm) while hydration increased significantly to 63 because of sweating caused by increased metabolic levels[48]. After 600 s, as the temperature began to fall down, sweat glands stopped secreting perspiration, and thus causing hydration to decrease to its initial value. On the other hand, heart rate showed a slight decrease and then a rapid increase up to 60 bpm, which was due to the fact that at the beginning of cooling, the temperature returned to a comfortable level and the subject's heart rate dropped to normal state. Nevertheless, as the temperature got colder, the subject's heart rate increased rapidly due to cold stress[49]. This test demonstrates that the EES can accurately track the changes in physiological parameters due to external changes.

Furthermore, the feasibility of EES in the diagnosis and screening of heart diseases in subjects with sinus arrhythmia was tested. Figure 4e, f shows the physiological information (i.e., mean P-R interval, and max ΔP-P interval over 5 cardiac cycles) extracted from V1–V6 ECGs of a subject with sinus arrhythmia. The ECG manifestations of wandering rhythm in the sinus node (also seen in normal subjects) are (1) the P wave remains sinus, i.e., the direction of the P wave does not change; (2) the PR interval is longer than 120 ms: Fig. 4e demonstrates the P-R interval acquired by EES and gel electrodes, respectively, and more consistent results are obtained on V1–V6; (3) the difference between the P-P intervals is longer than 120 ms. In lead V1, the difference between the longest P-P interval and the shortest P-P interval recorded by the EES over five cardiac cycles was 146 ms, which was close to the results of the gel electrode (140 ms). The results were essentially similar in the other leads, which were fluctuating (from 138 to 148 ms) but all longer than 120 ms, demonstrating the prospect of EES in screening and diagnosis of cardiac diseases such as sinus arrhythmias. The comparison with the gel electrode proves the accuracy of our EES in the precordial ECG, and can look forward to the further application of EES in portable heart disease diagnosis and treatment in the future.

DISCUSSION

We have successfully designed, fabricated, and applied a chest-scale, substrate-free EES with co-front-back compensation for 6-precordial-leads ECG and hydration monitoring. The filamentary serpentine design of the epidermal sensors has been demonstrated to be flexible without impeding perspiration and heat dissipation from the skin. The proposed co-front-back compensation method eliminates the unwanted signal from EEIs which cannot be directly filtered by software in back-end. With additional ECEs removed, the co-front-back compensation method is more conducive to wireless integration and wearability, and has higher compensation accuracy than the previous compensation. Epidermal sensing module and wireless DAQ module are integrated stably into a complete EES via liquid metal. Finally, the EES was applied and validated in different states of exercise, temperature stimulation, and sinus arrhythmia disease monitoring. It is worthwhile to expect that the self-adhesive hydrogel can be applied to improve the adhesion strength between EES and skin, especially under extreme conditions such as sweating, thus improving the robustness of the whole system. This EES has exhibited promising application prospects in personal health management, screening, and diagnosis of cardiac diseases, etc., and is expected to become an emerging medical-grade wearable ECG monitoring device.

METHODS

Preparation of EES

The EES consists of the epidermal sensing module and the soft wireless DAQ module. The epidermal sensing module is prepared with reference to our previous work[39]. The soft wireless DAQ module is fabricated by the FPCB process. The major components of the wireless DAQ module are listed in Supplementary Table 1. The epidermal sensing module and the soft wireless DAQ module were connected by a cushioning layer of liquid metal prepared as follows. A mold with the position of the wireless DAQ module hollowed was manufactured by 3D printing photosensitive resin. The mold was designed with tabs at the corresponding connection pads to form the holes, which were designed as cylinders with their diameter being 3 mm and depth being 2 mm. The liquid metal could be completely filled in the hole without dripping under the surface tension. After spraying with release agent (Ease Release 200, Smooth-On), Ecoflex (00-50, Smooth-On) was injected into the mold and left to cure in 25 °C for 6 h to obtain the Ecoflex sleeve with holes. The as-prepared Ecoflex sleeve was assembled together with the wireless DAQ module and the holes were filled with sufficient liquid metal, which should be 1–2 mm above the hole surface to make complete contact with the epidermal sensing module. The as-prepared Ecoflex sleeve is treated with a double-sided adhesive primer (TL-779, China) for 30 s to allow the double-sided adhesive (1509, 3 M) to adhere tightly to the Ecoflex. The double-sided adhesive, which is flexible and conformable to skin deformation (Supplementary Fig. 14), is cut to match the Ecoflex bonding surface. The wireless DAQ module with Ecoflex sleeve was attached to the corresponding position of the epidermal sensing module that has been transferred to the skin already by double-sided adhesive.

Simulation of the potential distribution in the skin

Considering skin as a two-dimensional mode, the thickness, the width, and the electrical conductivity of the dermis layer were set to 2 mm, 10 mm, 16 mS/m, respectively. The thickness and the electrical conductivity of the stratum corneum were set to 25 μm, 100 μS/m, respectively. The electrode was made of gold with thickness of 200 nm. Voltage sources of 40 mV, −70 mV, and −90 mV were set at the bottom of the dermis at the horizontal coordinates of 0 mm, 3.3 mm, and 10 mm. 40 mV and −90 mV correspond to the maximum and minimum action potentials, and −70 mV corresponds to the membrane potential of axons. The simulations were carried out in the commercial software COMSOL Multiphysics.

Validation of the co-front-back compensation strategy

The experiments were an analogy to our previous work[39]. The EWEs were attached on chest, while the EEIs were located on hands. EEIs were connected to EWEs. The ECEs required by the front-end compensation were attached on the right side of the abdomen, which is far from the heart and regarded as having stable electrical potential. The pure ECG, as the standard, was recorded directly on the chest. The uncompensated ECG was recorded from the electrodes simultaneously attached on hands and chest. The partially compensated ECG was recorded by introducing ECBs, which was parallel with and had the same length with ECBs. The signals recorded by the uncompensated channels and partially compensated channels were linearly combined by following the co-front-back compensation strategy. The muscles in hands were contracted by grasping a dynamometer and the EMG activated by muscles were recorded by EEIs and/or ECBs.

Heat distribution measurement

The participant's chest heat distribution was measured by an infrared radiometer (FLIR T630sc, USA), the lens of which is FOL 25 mm. The thermal image was imported into a commercial software FLIR. Two rectangle area measurement tools of the same size were applied to the thermal image in the left and right chest position, respectively. The rectangle was determined by two diagonal points, i.e., the nipple as well as the intersection of the epidermal sensing module and axillary midline. The average temperatures of each rectangle area were recorded for characterization.

Characterization of the hydration sensor

First, The moisturizing lotion was applied evenly on the arm skin, then the hydration sensor was attached. At this time, the hydration value of the skin would be at a high level due to the effect of the moisturizing lotion, and gradually decrease with time. After that, the impedance of both ends of the hydration sensor was scanned every 1 min (50–1000 Hz, step 50 Hz). The skin hydration value could be estimated by the correspondence between frequency and impedance[48]. The calculated hydration value was used to fit and calibrate the impedance of the hydration sensor at a given frequency (Supplementary Fig. 15).

Measurement of maximum adhesion force

For the adhesion force between the epidermal sensing module and the skin, a flat punch measurement was applied. An unpatterned, intact epidermal electronics were tailored to the same size as the punch (25 mm × 25 mm). The PET side of the tailored epidermal sensing module was firmly attached to the punch. Then press the skin vertically using the Au side of the punch that had the epidermal sensing module attached. The peeling test was carried out using a homemade peeling device. The skin was first pressed with a preload force of 2 N for 1 min, and then the punch was lifted at a rate of 30 mm min^{-1} to record the continuous peeling force in the process. The maximum adhesion force is recorded every 10 min.

Ethical information for studies involving human subjects

All experiments involving human subjects were conducted in compliance with the guidelines of Institutional Review Board. The Institutional Review Board of Tongji Hospital, Tongji Medical College, Huazhong University of Science and Technology approved the protocol of the study [permit number (2018) IEC (S512), Wuhan, China]. All participants for the studies were fully voluntary and submitted the written informed consents. All identifiable information was totally consented by the user.

DATA AVAILABILITY

Additional data related to this paper may be requested from the authors.

CODE AVAILABILITY

Code is available from the corresponding author upon reasonable request.

REFERENCES

1. Somers, M. P., Brady, W. J., Bateman, D. C., Mattu, A. & Perron, A. D. Additional electrocardiographic leads in the ED chest pain patient: right ventricular and posterior leads. *Am. J. Emerg. Med.* **21**, 563–573 (2003).
2. Teigeler, T. L., Ellenbogen, K. A. & Padala, S. K. The right-sided ECG for the right diagnosis. *Circulation* **138**, 107–109 (2018).
3. Zhang, Y., Sun, G. & Yang, Y. 12-lead ECG data acquisition system based on ADS1298. *Procedia Eng.* **29**, 2103–2108 (2012).
4. Vavrinsky, E. et al. Application of modern multi-sensor holter in diagnosis and treatment. *Sensors* **20**, 2663 (2012).
5. Jung, D. et al. Highly conductive and elastic nanomembrane for skin electronics. *Science* **373**, 1022–1026 (2021).
6. Mun, J. et al. A design strategy for high mobility stretchable polymer semi-conductors. *Nat. Commun.* **12**, 3572 (2021).
7. Yang, C. & Suo, Z. Hydrogel ionotronics. *Nat. Rev. Mater.* **3**, 125–142 (2018).
8. Xu, S. et al. Assembly of micro/nanomaterials into complex, three-dimensional architectures by compressive buckling. *Science* **347**, 154–159 (2015).
9. Fan, J. A. et al. Fractal design concepts for stretchable electronics. *Nat. Commun.* **5**, 3266 (2014).
10. Widlund, T., Yang, S., Hsu, Y.-Y. & Lu, N. Stretchability and compliance of free-standing serpentine-shaped ribbons. *Int. J. Solids Struct.* **51**, 4026–4037 (2014).
11. Kim, D.-H. et al. Epidermal electronics. *Science* **333**, 838–843 (2011).
12. Kwon, Y.-T. et al. Breathable, large-area epidermal electronic systems for recording electromyographic activity during operant conditioning of H-reflex. *Biosens. Bioelectron.* **165**, 112404 (2020).
13. Chung, H. U. et al. Binodal, wireless epidermal electronic systems with in-sensor analytics for neonatal intensive care. *Science* **363**, eaau0780 (2019).
14. Rogers, J. A., Chen, X. & Feng, X. Flexible hybrid electronics. *Adv. Mater.* **32**, 1905590 (2020).

15. Wang, Y. et al. All-weather, natural silent speech recognition via machine-learning-assisted tattoo-like electronics. *npj Flex. Electron* **5**, 20 (2021).

16. Wang, C. et al. Programmable and scalable transfer printing with high reliability and efficiency for flexible inorganic electronics. *Sci. Adv.* **6**, eabb2393 (2020).

17. Sim, K. et al. Three-dimensional curvy electronics created using conformal additive stamp printing. *Nat. Electron.* **2**, 471–479 (2019).

18. Ershad, F. et al. Ultra-conformal drawn-on-skin electronics for multifunctional motion artifact-free sensing and point-of-care treatment. *Nat. Commun.* **11**, 3823 (2020).

19. Zhang, L. et al. Wearable circuits sintered at room temperature directly on the skin surface for health monitoring. *ACS Appl. Mater. Interfaces* **12**, 45504–45515 (2020).

20. Lu, P. et al. Iontronic pressure sensor with high sensitivity and linear response over a wide pressure range based on soft micropillared electrodes. *Sci. Bull.* **66**, 1091–1100 (2021).

21. Yu, X. et al. Skin-integrated wireless haptic interfaces for virtual and augmented reality. *Nature* **575**, 473–479 (2019).

22. Zhang, B. et al. Breath-based human–machine interaction system using tribo-electric nanogenerator. *Nano Energy* **64**, 103953 (2019).

23. Zhuang, M. et al. Highly robust and wearable facial expression recognition via deep-learning-assisted, soft epidermal electronics. *Research* **2021**, 1–14 (2021).

24. Lim, H. et al. Advanced soft materials, sensor integrations, and applications of wearable flexible hybrid electronics in healthcare, energy, and environment. *Adv. Mater.* **32**, 1901924 (2020).

25. Hong, Y. J., Jeong, H., Cho, K. W., Lu, N. & Kim, D. Wearable and implantable devices for cardiovascular healthcare: from monitoring to therapy based on flexible and stretchable electronics. *Adv. Funct. Mater.* **29**, 1808247 (2019).

26. Han, M. et al. Catheter-integrated soft multilayer electronic arrays for multiplexed sensing and actuation during cardiac surgery. *Nat. Biomed. Eng.* **4**, 997–1009 (2020).

27. Kim, J. et al. Simultaneous monitoring of sweat and interstitial fluid using a single wearable biosensor platform. *Adv. Sci.* **5**, 1800880 (2018).

28. Yang, Y. et al. Wireless multilateral devices for optogenetic studies of individual and social behaviors. *Nat. Neurosci.* **24**, 1035–1045 (2021).

29. Grajales-Reyes, J. G. et al. Surgical implantation of wireless, battery-free optoelectronic epidural implants for optogenetic manipulation of spinal cord circuits in mice. *Nat. Protoc.* **16**, 3072–3088 (2021).

30. Lee, K. et al. Mechano-acoustic sensing of physiological processes and body motions via a soft wireless device placed at the suprasternal notch. *Nat. Biomed. Eng.* **4**, 148–158 (2020).

31. Capogrosso, M. et al. A brain–spine interface alleviating gait deficits after spinal cord injury in primates. *Nature* **539**, 284–288 (2016).

32. Yang, J. et al. Facile fabrication of robust and reusable PDMS supported graphene dry electrodes for wearable electrocardiogram monitoring. *Adv. Mater. Technol.* **6**, 2100262 (2021).

33. Tian, L. et al. Large-area MRI-compatible epidermal electronic interfaces for prosthetic control and cognitive monitoring. *Nat. Biomed. Eng.* **3**, 194–205 (2019).

34. Zhang, H. et al. A wearable 12-lead ECG acquisition system with fabric electrodes. in *2017 39th Annual International Conference of the IEEE Engineering in Medicine and Biology Society (EMBC)* 4439–4442 (2017).

35. Moin, A. et al. A wearable biosensing system with in-sensor adaptive machine learning for hand gesture recognition. *Nat. Electron.* **4**, 54–63 (2021).

36. Alberto, J. et al. Fully untethered battery-free biomonitoring electronic tattoo with wireless energy harvesting. *Sci. Rep.* **10**, 5539 (2020).

37. Yao, S. & Zhu, Y. Nanomaterial-enabled dry electrodes for electrophysiological sensing: a review. *JOM* **68**, 1145–1155 (2016).

38. Jeong, J.-W. et al. Materials and optimized designs for human-machine interfaces via epidermal electronics. *npj Flex. Electron* **2**, 6839–6846 (2018).

39. Wang, Y. et al. Electrically compensated, tattoo-like electrodes for epidermal electrophysiology at scale. *Sci. Adv.* **6**, eabd0996 (2020).

40. Huang, Z. et al. Three-dimensional integrated stretchable electronics. *Nat. Electron.* **1**, 473–480 (2018).

41. Ha, T. et al. A chest-laminated ultrathin and stretchable E-tattoo for the measurement of electrocardiogram, seismocardiogram, and cardiac time intervals. *Adv. Sci.* **6**, 1900290 (2019).

42. Oh, E. et al. Highly reliable liquid metal-solid metal contacts with a corrugated single-walled carbon nanotube diffusion barrier for stretchable electronics. *Adv. Funct. Mater.* **28**, 1806014 (2018).

43. Secor, E. B., Cook, A. B., Tabor, C. E. & Hersam, M. C. Wiring up liquid metal: stable and robust electrical contacts enabled by printable graphene inks. *Adv. Electron. Mater.* **4**, 1700483 (2018).

44. Chi, Y. M., Jung, T.-P. & Cauwenberghs, G. Dry-contact and noncontact biopotential electrodes: methodological review. *IEEE Rev. Biomed. Eng.* **3**, 106–119 (2010).

45. Heikenfeld, J. et al. Wearable sensors: modalities, challenges, and prospects. *Lab. Chip* **18**, 217–248 (2018).

46. Yang, S. et al. "cut-and-paste" manufacture of multiparametric epidermal sensor systems. *Adv. Mater.* **27**, 6423–6430 (2015).

47. Yang, X. et al. Ultrathin, stretchable, and breathable epidermal electronics based on a facile bubble blowing method. *Adv. Electron. Mater.* **6**, 2000306 (2020).

48. Wang, Y. et al. Low-cost, μm-thick, tape-free electronic tattoo sensors with minimized motion and sweat artifacts. *npj Flex. Electron* **2**, 6 (2018).

49. Huang, C.-M. et al. Radial pressure pulse and heart rate variability in heat- and cold-stressed humans. *Evid. Based Complement. Altern. Med.* **2011**, 1–9 (2011).

ACKNOWLEDGEMENTS

AUTHOR CONTRIBUTIONS

The design, preparation, and characterizations of epidermal sensing module were completed by L.Y., Y.W., C.H., J.W., R.H., and Y.W.; the development of wireless DAQ module were completed by L.Y., J.Z., and Y.W.; the simulation of the potential distribution in the skin was carried out by Y.W.; the development and experimental validation of the co-front-back compensation strategy were implemented by Y.W., Y.A.H., L.Y., Y.B., and C.H.; the typical application of EES was carried out by L.Y., Y.W., Y.B., and Y.W.; Y.A.H., Y.W., and L.Y. contributed to the writing of the manuscript; Y.A.H. supervised the overall research.

COMPETING INTERESTS

The authors declare no competing interests.

ADDITIONAL INFORMATION

Supplementary information The online version contains supplementary material available at https://doi.org/10.1038/s41528-022-00159-7.

Correspondence and requests for materials should be addressed to YongAn Huang.

Reprints and permission information is available at http://www.nature.com/reprints

Publisher's note Springer Nature remains neutral with regard to jurisdictional claims in published maps and institutional affiliations.